

Supporting Information

Marlon *et al.* 10.1073/pnas.0808212106

SI Methods

This file contains additional methodological details, 1 table that describes the sites in the main text, and 3 figures. Fig. S1 is a site map. Fig. S2 shows the individual records of charcoal influx and proportions of arboreal pollen during deglaciation along with background trends in biomass burning and radiocarbon dates. Fig. S3 shows the peak frequencies and magnitudes of the high-resolution sites, as well as the number and location of radiocarbon dates in these records.

Data Sources and Locations. Charcoal and pollen data sources, site locations and elevation, and temporal coverage during the Last Glacial–Interglacial Transition (LGIT) are provided in Table S1. Numbers in parentheses after site names are reference numbers. Site locations are shown in Fig. S1 and are coded to reflect the existence of a charcoal peak at 12.9 and 11.7 ka, as determined by the analysis techniques described below.

Chronologies. Lake-sediment records of the kind selected for paleoecological studies have generally well-behaved sedimentation regimes with slowly varying sedimentation rates. This allows chronological control with fewer radiocarbon dates than required for discontinuous terrestrial records, or marine records with continuous or intermittent bioturbation of sediments. For example, the age of a synchronous vegetation change in eastern North America, the *Tsuga* (hemlock) decline, can be estimated with subcentury precision (4750 ¹⁴C y BP, with a standard error of the mean of ≈ 50 y) using networks of lake records like those used here (1, 2). However, owing to the reorganizations of the circulation of the atmosphere and ocean that are involved in the abrupt climate changes, larger than usual uncertainties arise in calibrating radiocarbon ages during the LGIT (3), and so we compared the results from our peak identification analysis based on both a narrow 100-y and wider 500-y window width. As described in the main text, peaks were not more likely to occur at 12.9 than at 11.7 ka in either case.

Analysis of Individual Charcoal and Pollen Records. Charcoal concentration data (particles cm^{-3}) were converted to influx values (particles $\text{cm}^{-2} \text{y}^{-1}$) by dividing charcoal values by sample deposition times (y cm^{-1}). For the low-resolution records (>50 y sample^{-1}), we used quantile regression to estimate background charcoal influx values as the 50th percentile (4). The degrees of freedom parameter (df) was 10 for all but 3 records (i.e., 73 for East Lake, 50 for Sharkey Lake, and 6 for Walker Lake).

In continuously sampled (high-resolution), macroscopic (typically $>100 \mu\text{m}$) charcoal records, large charcoal peaks above background represent individual, local fire events or clusters of events (fire episodes) as has been demonstrated by examination of the portions of the sedimentary records that overlap with dendrochronological or historical records of fire (5, 6). Lower-resolution records based on microscopic charcoal ($<100 \mu\text{m}$), reflects burning at broader scales (7). Low-resolution records will integrate individual fire episodes, but increased fire activity can still be inferred from large peaks in low-resolution records (8). For Fig. 2 in the main text, any increase in charcoal influx above background within a defined time period (i.e., either ± 50 or ± 250 y) was considered a “peak.”

The high-resolution (<50 y per sample) charcoal influx series were decomposed into background and peaks components using CharAnalysis (9), which allows us to reconstruct peak frequencies and to quantify peak sizes in addition to separating peaks

from background charcoal levels (Fig. S3). Charcoal values were interpolated to constant time intervals based on the median resolution at each site. A robust lowess smoother was used to define background trends with a 500-y window width for all but 2 records (sites 18 and 13), which showed an improved signal-to-noise ratio with larger window widths (18). Site 18 was smoothed with a 600-y window and site 13 was smoothed with an 800-y window. Peaks were identified by calculating the residuals above a locally defined threshold. The peaks component was defined as the residuals after subtracting background values from the interpolated series, and charcoal peaks were identified by calculating a locally defined threshold value separating fire-related and non-fire-related variations in the peaks component (9). Only peaks that had a maximum charcoal count with a $<5\%$ chance of coming from the same Poisson distribution as minimum charcoal counts within the previous 75 y were considered, except for site 13, 20, and 24, where all peaks were counted due to the lack of the sample volume information required to perform the minimum count test (9, 10). Peak magnitudes were obtained by calculating the positive deviations above the background. Ratios of arboreal to nonarboreal pollen percentages (AP/NAP) were obtained by dividing the sum of arboreal and shrub pollen percentages (AP) by the sum of the total terrestrial pollen percentage $[\text{AP}/(\text{AP} + \text{NAP})]$. Changes in AP were used as an indicator of major changes in woody fuel levels, not as a tool for reconstructing detailed changes in vegetation community composition, which is beyond the scope of this article.

Trends in Charcoal Influx, Peak Frequency, and Arboreal Pollen. The estimation of trends in noisy data like the charcoal influx data involves a tradeoff between (i) fitting a relatively simple model, like a straight line or polynomial, which allows assessment of the significance of the trend to be made (11) and (ii) using a more flexible or “data-adaptive” model which may better represent more complicated or nonlinear forms of a trend, but which makes it harder to establish the overall significance of the trend (12). We use 2 approaches here: (i) a piecewise linear or segmented-regression model, which allows some flexibility in the fitted model, in particular changes in slope and intercept at some (possibly unknown) breakpoints, and (ii) a local regression or “lowess” approach, which makes no assumptions about the form of the overall trend.

The charcoal influx data were first transformed using the Box–Cox transformation to stabilize the variance of the data as described in Power *et al.* (13). The transformed values were converted to Z scores by subtracting the mean value and dividing by the standard deviation using a base period of 15–10 ka to allow comparisons among the records that feature widely varying average charcoal influx rates.

We used the “segmented” package (14) from the R-Project (15) to fit an overall linear trend to the charcoal influx data, allowing for changes in the slope and intercept of the trend line at several breakpoints, which were simultaneously estimated with the trend. There is a tradeoff between the number of breakpoints (and the length of the intervals they define) and the interpretability and robustness of the results. Too few breakpoints may lead to a less-good fit to the data, and greater heterogeneity of the intervals or episodes that are defined, whereas too many breakpoints lead to more complicated ad hoc interpretations of the results and to greater sensitivity of the results to the specific data being analyzed. We explored linear and polynomial (2nd- and 3rd-order) trends, and 2–4 break-

points, with starting values for the breakpoints at even 1,000-y intervals from 11,000 to 14,000 y BP.

The best-fitting model with the fewest parameters was a segmented straight-line model with breakpoints at 12,820 y BP (SE = 128.0 y) and 11,550 yr BP (SE = 162.3 y). Because these breakpoint ages are indistinguishable from the beginning and end of the YDC (12,875 y BP and 11,660 y BP, respectively), we refit this model using the latter values as breakpoints using ordinary least squares “dummy variable” regression. This model is:

$$\begin{aligned} \text{Influx} &= 5.241697 - 0.000452 \cdot \text{Age} && (\text{Age} < 11,660 \text{ y BP}) \\ & [0.569100] [0.000053] \\ &= -0.797223 + 0.000071 \cdot \text{Age} && (11,600\text{--}12,875 \text{ y BP}) \\ & [1.034000] [0.000084] \\ &= 6.610190 - 0.000512 \cdot \text{Age} && (>12,875 \text{ y BP}) \\ & [0.625000] [0.000045]. \end{aligned}$$

where the values in square brackets are the standard errors of the regression coefficients, and $F = 137$ ($P < 2.2 \times 10^{-16}$), $R^2 = 0.1647$. Note that the slopes of the line segments before (-0.000452) and after (-0.000512) the YDC are virtually identical, but fitting a model that constrains them to be so adds little to the efficiency of the model. Note also that the slope of the line segment during the YDC is not significantly different from zero. This model yields the straight-line segments on Fig. 1C, and demonstrates the statistical significance of the overall trend in charcoal influx over the LGIT as well as the absence of a trend during the YDC.

A local-regression or lowess curve (16) was also fit to the data to show the long-term trends unconstrained by the specification of a particular model of the trend. The lowess curve-fitting procedure used the tricube weight function with a fixed-width window of 200 y (100-y half-width) as opposed to a variable-width window that “spans” a fixed proportion of the data points. Fitted values were obtained at “target points” spaced 10 y apart. (Note that this interval is not an expression of our belief in the chronological precision of the data, but simply allows us to graph the fitted values in a reasonable way.) A robustness iteration was used to minimize the influence of unusual points or outliers. We also calculated bootstrap confidence intervals for the lowess

curve (1,000 replications) where the sampling-with-replacement was done by sites as opposed to individual samples, to assess the impact of the inclusion or exclusion of specific sites in our dataset. The lowest fitted values appear as the smooth curve in Fig. 1C, and the 5th and 95th percentiles of the bootstrapped fitted values define the shaded bands. Note that the segmented-regression trend model and the lowess curve describe the same general trend in charcoal influx during the LGIT.

The density of charcoal peaks in the high-resolution charcoal records (Fig. 1D) was displayed by using a kernel density-estimator (17). We selected a bandwidth of 100 y, which provides a compromise between oversmoothing the peak frequencies while still displaying local maxima in peak frequencies that are supported by peaks in multiple individual records. Bootstrap confidence intervals were obtained in the same way as for the influx data.

AP proportions were transformed using the “angular” or arcsine transformation, and a composite curve (Fig. 1E) was constructed by smoothing the transformed data in a similar fashion as the charcoal influx data. However, because the temporal resolution of the pollen data are typically less than that of the charcoal data, we used a larger window width (200-y half-width) to smooth these data. Bootstrap confidence intervals were again obtained as for charcoal influx.

The Increase in Charcoal at 13.2 ka. The charcoal increase at 13.2 ka is evident in 14 of the 33 sites recording fires by 13.1 ka (sites 1, 2, 10, 15, 17, 18, 19, 20, 21, 22, 23, 26, 30, and 35; Fig. S2) from 8 different regions. These sites span an elevation range of 8–2,863 m, with 5 sites located above 2,000 m. Similar increases in charcoal influx occurred previously at 3 sites (sites 2, 19, and 21), so the change was unprecedented in only 11 records. Of these 11 records, 13.2 ka marks the beginning of a discrete peak at 7 of them (sites 1, 15, 17, 18, 23, 26, and 30), versus an increase in baseline levels at the remaining 4 sites (sites 10, 20, 22, and 35). Fire frequency also increased to a local maximum at 13.2 ka, after a peak in AP at 13.4 ka (Fig. 2). In contrast, 20 sites show low charcoal influx at 13.2 ka, illustrating that burning was widespread, but not continent-wide at the time.

- Webb T, III (1982) in *Third North American Paleontological Convention Proceedings* (Montreal), pp 569–572.
- Bennett KD, Fuller JL (2002) Determining the age of the mid-Holocene *Tsuga canadensis* (hemlock) decline, eastern North America. *Holocene* 12:421–429.
- Muscheler R, et al. (2008) Tree rings and ice cores reveal C-14 calibration uncertainties during the Younger Dryas. *Nat Geosci* 1:263–267.
- Koenker R (2005) *Quantile Regression* (Cambridge Univ Press, Cambridge, UK).
- Clark JS (1990) Fire and climate change during the last 750 yr in northwestern Minnesota. *Ecol Monogr* 60:135–159.
- Whitlock C, Bartlein PJ (2004) in *Developments in Quaternary Science* (Elsevier, Amsterdam).
- Patterson WA, Edwards KJ, Maguire DJ (1987) Microscopic charcoal as a fossil indicator of fire. *Quat Sci Rev* 6:3–23.
- Carcaillet C, et al. (2001) Change of fire frequency in the eastern Canadian boreal forests during the Holocene: Does vegetation composition or climate trigger the fire regime? *J Ecol* 89:930–946.
- Higuera PE, et al. (2008) Frequent fires in ancient shrub tundra: Implications of paleo-records for Arctic environmental change. *PLoS ONE* 3:e0001744.
- Gavin DG, Hu FS, Lertzman K, Corbett P (2006) Weak climatic control of stand-scale fire history during the late Holocene. *Ecology* 87:1722–1732.
- Wigley TML (2006) in *A Report by the Climate Change Science Program and the Subcommittee on Global Change Research*, eds Karl TR, Hassol SJ, Miller CD, Murray WL (U.S. Climate Change Science Program, Washington, DC), pp 129–139.
- Harvey DI, Mills TC (2003) Modelling trends in Central England temperatures. *J Forecasting* 22:5–47.
- Power MJ, et al. (2007) Changes in fire regimes since the Last Glacial Maximum: an assessment based on a global synthesis and analysis of charcoal data. *Clim Dynam* 30:887–907.
- Muggeo VMR (2008) Segmented: Segmented Relationships in Regression Models (R Package), Version 0.2-4.
- R Development Core Team (2008) R: A Language and Environment for Statistical Computing (R Foundation for Statistical Computing, Vienna), Version 2.8.0. Available at <http://www.R-project.org>.
- Cleveland WS, Devlin SJ (1988) Locally weighted regression: an approach to regression analysis by local fitting. *J Am Stat Assoc* 83:596–610.
- Venables WN, Ripley BD (2002) *Modern Applied Statistics with S* (Springer, New York).
- Higuera PE, Brubaker LB, Anderson PM, Hu FS, Brown TA (2009) Vegetation mediated the impacts of postglacial climate change on fire regimes in the southcentral Brooks Range, Alaska. *Ecological Monographs*, in press.

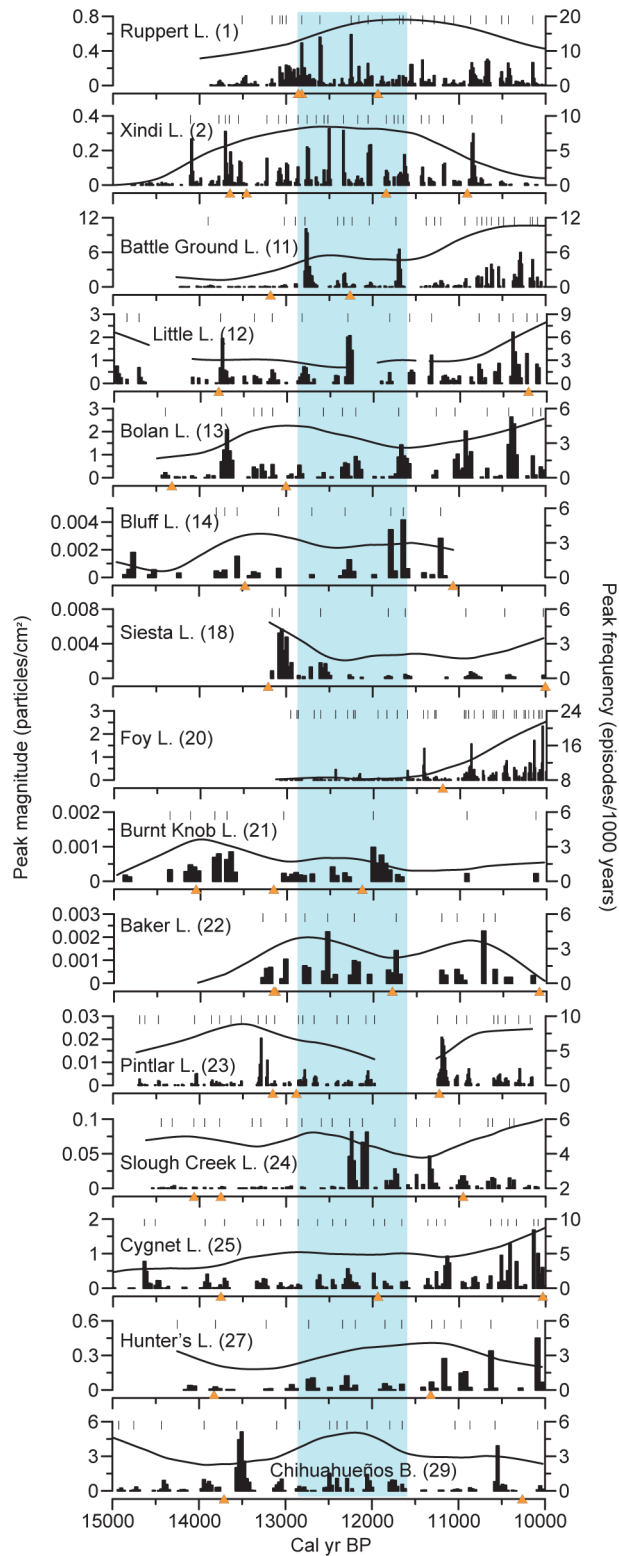


Fig. S3. Fire-regime reconstructions, including peak episodes (tic marks), peak frequencies (smooth black line), and positive deviations above background or peak magnitudes from high-resolution North American charcoal records during deglaciation. Orange triangles are radiocarbon or tephra dates. The Younger Dryas interval is shaded blue.

